Environmental Processes (2021) 8:1027–1045
https://doi.org/10.1007/s40710-021-00524-0

ORIGINAL ARTICLE

Correlation Wavelet Analysis for Linkage between Winter Precipitation and Three Oceanic Sources in Iran

Atefe Ebrahimi[1] · **Dariush Rahimi**[1] · **Mohammad Joghataei**[2] · **Saeed Movahedi**[1]

Received: 23 December 2020 / Accepted: 18 May 2021/

Abstract
This paper aims to find the possible relationships between winter precipitation (December, January, February; DJF) in Iran with three oceanic sources through the correlation wavelet analysis by applying the continuous wavelet transform (CWT), the cross–wavelet transform (XWT), and the wavelet transform coherence (WTC). The sources in the North Atlantic Ocean (30°W-70°W, 10°N-30°N), the South Pacific Ocean (80°W-120°W, 20°S-40°S) and the Indian Ocean (50°E-100°E, 10°S-40°S) were selected using Pearson correlation coefficient ($PCC > 0.5$) that can represent the possible relationships between Iran's winter precipitations with the oceanic sea surface temperature (SST) anomaly. The monthly gridded precipitation and SST data with a $2.5° \times 2.5°$ resolution were evaluated from 1984 to 2019 to achieve this goal. The XWT results of precipitation and SST anomaly showed that the 8–16 months period is the most effective and predominant period between the South Pacific Ocean and 81% of all the precipitation zones. WTC results for the North Atlantic Ocean and 72% of all the precipitation zones showed periods of 4–8 (36%) and 16–32 (36%) months as the dominant duration. Despite the proximity of the Indian Ocean to the precipitation zones, there is no significant causal relationship between them, based on the XWT results. However, due to Madden–Julian oscillation (MJO), the 4–8 months period (45%) was seen between the Indian Ocean and some precipitation zones, based on WTC results.

Keywords Cross wavelet transform (XWT) · Wavelet transform coherence (WTC) · Correlation wavelet analysis · Sea surface temperature (SST) · Oceanic sources

---

✉ Dariush Rahimi
d.rahimi@geo.ui.ac.ir

✉ Mohammad Joghataei
mjoghataei@yazd.ac.ir

Extended author information available on the last page of the article

1 Introduction

The most critical dynamic property of the atmosphere is the ability to hold various wave motions in the spatiotemporal domain that can interact through complex nonlinear effects. Statistical analysis of the precipitation data can determine the complexity through correlation analysis and dominant frequency detection. Precipitation plays an essential role in the climatological study of arid and semiarid regions, because lack of precipitation leads to a deficit of surface and groundwater resources (Shamshirband et al. 2020). Iran is located in an arid and semiarid region where precipitation variability and fluctuations are intrinsic features. Therefore, water resources management and the socio-economic effects of climate change are the critical challenges throughout Iran (Farajzadeh and Alizadeh 2018; Raziei et al. 2009). Iran has been subject to successive droughts or devastating floods over recent years. Flash floods associated with extreme rain events are a major hydrological disaster in Iran's central plateau due to the region's unique topographic features and the high occurrence frequency of such calamities (Rousta et al. 2016).

Today, researchers commonly use new methods to estimate and predict climate parameters, such as precipitation, evaporation (Barbulescu 2016; Moazenzadeh et al. 2018; Sattari et al. 2020). Wavelet transform (WT) is one of these new methods used to create a good representation of the signal in both time and frequency domains (Partal and Cigizoglu 2009; Partal and Kisi 2007). The wavelet is an accepted tool in signal processing and was developed by Grossmann and Morlet (1984). In recent decades, wavelet transform has become a beneficial technique for analyzing variations, dominant periods, and time series trends. Wavelet transform has some benefits over Fourier transform, such as the capability to analyze signals at the multi-time frequency domain. The WT is an efficient tool to process time-series data with nonstationary characteristics occurring over limited spatiotemporal domains. The disintegration of a time series into time-frequency space can determine the dominant modes of variability and how those modes vary in time (Kisi and Shiri 2011; Nazari-Sharabian and Karakouzian 2020; Torrence and Compo 1998; Xu et al. 2005).

Wavelet analysis has been widely used in different research studies worldwide to quantify streamflow variability or groundwater (Chen et al. 2016; Coulibaly and Burn 2004; Qi et al. 2018; Smith et al. 1998), to analyze temperature time series (Araghi et al. 2015; Das et al. 2020; Chellali et al. 2010), or to predict time series (Azad et al. 2015; Guntu et al. 2020). This method has also been used to analyze precipitation events and their teleconnection with large-scale climate (Canchala et al. 2020; Hermida et al. 2015; Jiang et al. 2014; Tan et al. 2016), and to analyze monthly and seasonal precipitation (Coulibaly 2006; Chandran et al. 2016; Fritier et al. 2012; Kim 2004; Li and He 2017; Pathak et al. 2016; Rehman et al. 2019; Santos et al. 2003).

Previous research on Iran showed that different teleconnections, such as the Arctic Oscillation (AO), the North Atlantic Oscillation (NAO), and the Quasi-Biennial-Oscillation (QBO), could affect hydrological cycles and precipitation (Ahmadi et al. 2019; Helali et al. 2020; Kalimeris et al. 2017; Lee et al. 2018). Researchers have not only performed various spatiotemporal statistical analyses of precipitation in Iran (Amiri et al. 2017; Amiri et al. 2016; Amiri and Conoscenti 2017; Amiri and Mesgari 2016, 2017, 2019) but also have conducted different wavelet analyses focusing on precipitation (Amiri et al. 2016; Araghi et al. 2017; komasi et al. 2018; Nourani et al. 2009; Roushangar and Alizadeh 2018; Roushangar et al. 2018; Shafaei et al. 2016). As of today, and to the best knowledge of the authors, no study has used wavelet analysis to investigate the causal relationship between precipitation and a controlling climate parameter.

The effect of sea surface temperature (SST) on precipitation is not limited to coastal areas and can also affect areas far from the sea. Research has shown that changes in the SST of water sources can significantly affect precipitation fluctuations in other areas (Mechoso et al. 1990; Moron et al. 2001; Nicholls 1989; Streten 1983; Uvo et al. 1998; van der Ent and Savenije 2013). Some other regional studies rely on wavelet analysis to study the relationship between precipitation and the oceanic sources of SST (Kuo et al. 2010; Mwale et al. 2007). This paper initially identified homogeneous precipitation zones. Unlike previous studies that have worked on known indicators, this study identified three oceanic sources, including the North Atlantic, South Pacific, and the Indian Oceans, using correlation analysis, with high correlation coefficients and dependency on the different zones. Next, the XWT and WTC were used to determine the time-frequency and temporal lag between SST and winter precipitation in Iran. This research can be used for the estimation of monthly and seasonal precipitation variability in Iran.

The primary goal of this study is to investigate interaction within a time-frequency domain among Iran's winter precipitations and three oceanic sources worldwide. This paper comprises the following sections: The first section gives a brief overview of the previous research, and the second section presents a case study and relevant data combined with a complete description of the methodology. The results and discussion are outlined in the third section, followed by the conclusions in the final section.

2 Materials and Methods

2.1 Case Study and Data

The study used the monthly mean SST of global gridded data from the National Center for Environmental Prediction-National Center for Atmospheric Research (NCEP/NCAR Reanalysis) (Kaplan et al. 1998) and obtained the monthly mean precipitation data in Iran with 2.5° × 2.5° resolution from the Global Precipitation Analysis Products (GPCC) full data Monthly Product Version 2020 (Schneider et al. 2020) between 1984 and 2019. Based on this data, 26 grid points are located in Iran (Fig. 1a). The anomalies data are calculated by removing the seasonal cycle averaged over the thirty-year period. Note that the winter is the rainy season in Iran and that almost throughout Iran, more than half of the annual precipitation occurs in winter (Darand and Mansouri Daneshvar 2014; Domroes et al. 1998; Khalili et al. 2016). Therefore, this study relied on precipitation data from December, January and February (DJF).

Based on this data, 26 grid points are located in Iran. The analogous area was identified using correlation analysis. The area comprised 11 rainfall areas. The first zone includes the valley of the Aras River and the border between Nakhjivan and Armenia. Zone 2 is characterized by relatively high precipitation amounts (about 400 mm yearly). Zone 3 is the vastest area with annual precipitation of 250–1000 mm. Zone 4 corresponds to the western Alborz and southern coasts of the Caspian Sea. High annual precipitation in this zone is due to being on Siberian high pressure and the Caspian Sea water source. The next zone (zone 5) is located on the southern slopes of the Alborz mountains. Zone 6 conforms to the South Zagros mountains in the Khuzestan Plain, and STHP affects this zone. Zone 7 is placed on the northern border of the Dasht-e-Kavir. Zone 8 grabs the North-East of Iran, and Zone 9 is formed by the Oman Sea coastal area. Finally, Zone 10 includes the Lut desert with extremely infrequent precipitation over the entire year. The zone 11 is set in the South-East of Iran and is firmly influenced by monsoon (Fig. 1a; Table 1).

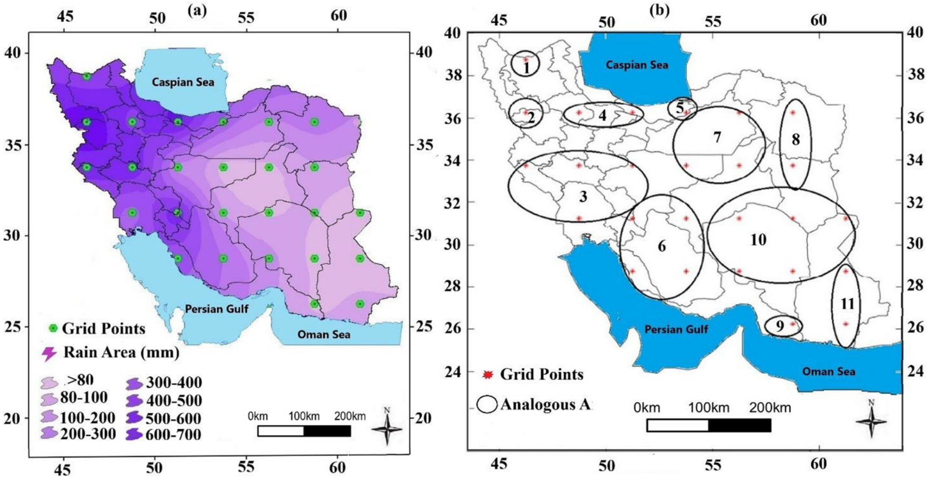

Fig.1 (**a**) Map of Iran illustrating the position of grid points; (**b**) Precipitation zones of Iran

Iran is approximately located between 25°N and 40°N in latitude and between 44°E and 64°E in longitude. Based on the Koppen climate classification, most parts of Iran are categorized as generally arid (BW) and semiarid (BS) climates (Tabari and Talaee 2011). The mean annual precipitation of Iran is about 241 mm. Half of the annual precipitation occurs in winter. The coefficient of annual precipitation variations varies from 18% in the north to 75% in southeast Iran (Dinpashoh 2006). The Caspian Sea coastal areas and the country's northern and north-western areas are subjected to higher precipitation. As seen in Fig. 1b, the southern, eastern, and central desert zones display the lowest annual precipitation values (Ashraf et al. 2013).

2.2 Methods

The methodology in this paper consists of correlation and wavelet transform. The researchers used the Pearson correlation to obtain the three oceanic sources. The research steps included: determining precipitation zones, identifying three oceanic regions showing the highest correlation with precipitation, and finding the temporal pattern and lags between winter precipitation and SST of three oceans globally (Fig. 2).

Table 1 Overall summary of geographical characteristics of precipitation zones of Iran

Zone ID	Annual Precipitation(mm)	Geography Location	Climate
1	250–600	Aras Basin(NW of Iran)	Humid
2	280–850	Urmia Basin	Humid
3	250–1400	Zagros Mountain	Humid
4	250–500	South slop Alborz mountain	Semiarid
5	650–1500	Caspian Sea coast	Humid
6	150–300	Khuzestan plain-Bandar-Abbas	Semiarid
7	100–300	Central mountain and desert	Arid
8	100–250	North-East (Khorasan)	Semi-arid
9	100–200	North Oman Sea	Arid
10	30–100	Lut and Dasht Kavir	Arid
11	80–200	South-East of Iran (Sistan-Balochistan)	Arid

In a broad sense, the Pearson correlation coefficient (PCC) is a measure of an association between variables. In the correlated data, a variable correlate with another variable, either in its positive or negative direction. The coefficients here are scaled within the −1 to +1 range, where 0 indicates the absence of any linear or monotonic association (Schober et al. 2018). Bravais first found this correlation coefficient in 1846, and Karl Pearson was the first one to describe its standard technique for calculation in 1896. Pearson's correlation coefficient is a measure of the strength in the linear relevance between two variables (Hauke and Kossowski 2011) expressed as follows:

$$r = \frac{N\sum xy-(\sum x)(\sum y)}{\sqrt{\left\{N\sum x^2-(\sum x)2\right\}\{N\sum y^2-(\sum y)2\}}} \tag{1}$$

where N is the number of pairs of values, $\sum x$ is the sum of the x values, and $\sum y$ is the sum of the y values (Obilor and Amadi 2018).

2.2.1 Wavelet Analysis

Several methods, such as Fourier analysis, apply to operating signal and time series analysis. The majority of these methods are mathematical transforms that turn vectors or functions from one space to another. Wavelet transform is a powerful mathematical transformation widely used for signal processing. The WT is an analytical instrument, providing a time-frequency presentation of a signal in the time domain (Araghi et al. 2017; Komasi et al. 2018).

Continuous Wavelet Transform (CWT) of a time series (x_n, $n = 1, \ldots, N$) with uniform time steps δt is defined as the convolution of x_n with the scaled and normalized wavelet as follows (Grinsted et al. 2004):

$$w_n^X(s) = \sqrt{\frac{\delta t}{s}}\sum_{n'=1}^{N} x_{n'}\psi_o\left[\left(n'-n\right)\frac{\delta t}{s}\right] \tag{2}$$

where n is the localized time index, n' is the time variable, s is the wavelet scale, δt is the sampling period, N is the number of points in the time series.

Cross Wavelet Transform (XWT) shows that regions in time frequency space with common power have a stable phase relationship, which links the time series. The cross wavelet transform of the time series X_n and Y_n is defined as:

$$W^{(xy)} = W^{(x)}W^{(y*)} \tag{3}$$

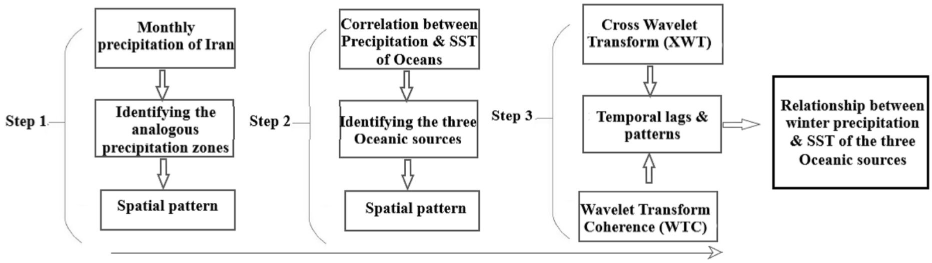

Fig. 2 The schematic framework of the methodology used in this study

where W^{xy} is the cross wavelet power, according to Grinsted et al. (2004). The theoretical distribution of the XWT of two time series with background power spectra P_k^x and P_k^y are given by Torrence and Compo (1998) as:

$$D\left(\frac{\left|W_n^X(S)W_n^{y^*}(S)\right|}{\sigma_X\sigma_Y} < P\right) = \frac{Z_v(p)}{v}\sqrt{P_k^X P_k^Y} \tag{4}$$

where $\sigma_X$and $\sigma_Y$are the respective standard deviations, and $z_v(p)$ is the confidence level associated with the probability p for a probability density function (pdf) is defined by the square root of the product of two x^2distributions. For $v = 1$ (real wavelets), Z_1 (95%) = 2.182, while for $v = 2$ (complex wavelets), a 5% significance level is also calculated exerting $Z_2 = 3.999$ (Torrence and Compo 1998; Grinsted et al. 2004).

Wavelet Transform Coherency (WTC) discovers regions in the time-frequency space with two different time series that are not necessarily powerful. A useful measure is how coherent the cross wavelet transform is in the time-frequency space. The wavelet coherence of time series is defined as:

$$R_n^2(S) = \frac{\left|S\left(S^{-1}W_n^{XY}(S)\right)\right|^2}{S\left(S^{-1}\left|S\left(W_n^x(S)\right|^2\right)\cdot S\left(S^{-1}\left|S\left(W_n^y(S)\right)\right|^2\right.\right.} \tag{5}$$

where $R_n^2(S)$ changes between 0 and 1. Given the two-time series X and Y, with wavelet transforms $W_n^x(S)$ and $W_n^y(S)$ where n is the time index, S is a smoothing operator. It is helpful to use the wavelet coherence as a localized correlation coefficient in the time-frequency space. The smoothing operator S is written as:

$$S(W) = S_{scale}(S_{time}(W_n(s))) \tag{6}$$

It is clear S_{scale} defines smoothing along the wavelet scale, and S_{time} does it in the time axis. Based on Torrence and Webster (1999), a suitable smoothing operator for the Morlet wavelet can be seen in the following two equations:

$$S_{time}(W)\Big|S = \left(W_n(S)\cdot S_1^{\frac{-1^2}{2S^2}}\right)\Big|S \tag{7}$$

$$S_{time}(W)|S = (W_n(S)\cdot C_2\Pi(0.6S))|n \tag{8}$$

where C_1 and C_2 are used in the normalization process, and Π is used as the rectangle function. The factor of 0.6 is the experimentally specified scale decorrelation length for the Morlet wavelet (Araghi et al. 2017; Grinsted et al. 2004; Torrence and Compo 1998; Torrence and Webster 1999). There are several points to consider in interpreting wavelet analysis: The thick black contour specifies the 5% significance level. The cone of influence (COI) where edge effects might skew the picture is shown as a lighter shading, and finally, the relative phase communication is marked as arrows, with in-phase pointing right, anti-phase pointing left. Arrows pointing in other directions indicate that SST anomaly leads to winter precipitation (Grinsted et al. 2004; Roushangar et al. 2018). Warmer colors (e.g., yellow and red) display stronger correlations, while colder colors (e.g., blue) indicate weaker correlations (Nazari-Sharabian and Karakouzian 2020).

3 Results and Discussion

3.1 Spatial Correlation Pattern

Initially, the PCC between the precipitation zones and SST of the oceans was calculated to obtain the oceanic sources influencing Iran's winter precipitation. Figure 3 shows the correlation of the oceanic regions with Iran's winter precipitation in zones 3, 4, 6, and 8. Note that because of the large number of maps, Fig. 3 presents the correlation between four precipitation zones and other maps are included in the Supplementary Materials (SM) file (See Figs. SM1 to SM7). The results show that all precipitation zones in Iran correlate with one of the three regions: The North Atlantic (East-North of America) (30°W-70°W, 10°N-30°N), the South Pacific (West-South of America) (80°W-120° W, 20°S-40° S), and the Indian Ocean (50°E-100°E, 10°S-40°S). The PCCs of these regions were above 0.5, and the yellow and blue in Fig. 3 respectively indicate a positive and negative correlation.

3.2 Wavelet Analysis Patterns

After determining the three oceanic sources, the study used the CWT to determine the significant periodic characteristics of the data series. Furthermore, the XWT and WTC were used to determine the time-frequency between each of these three regions and the eleven precipitation zones in Iran. The CWT was used to check for significant periodic characteristics of data series. Despite the main focus on winter precipitation, in the CWT section, precipitation data were used for the whole year of the statistical period. The wavelet power spectrum plots showed that some periodic events affected the annual total precipitation series trend in Iran's precipitation zones. As seen in Fig. 4, spectral analysis shows a continuous wavelet for the 11 rainfall regions of Iran. In almost all regions within the bands between 36 to 84 months, the El Niño Southern Oscillation (ENSO) effects on the precipitation were apparent (Bruun et al. 2017; Muhati et al. 2007). Return periods of 2 to 3 years, which can be attributed to the QBO, were seen in zones 4, 5, 6, 7, and 8 (Baldwin et al. 2001; Randel et al. 1999). In zones number

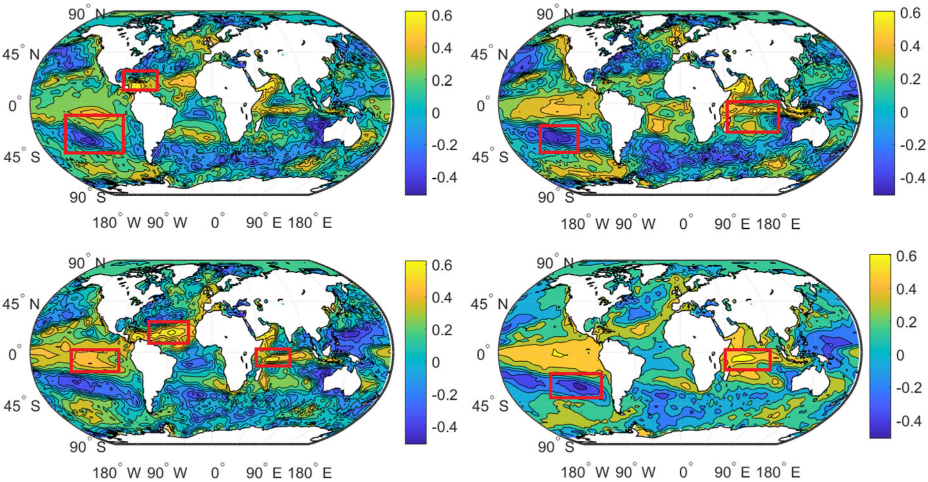

Fig. 3 Correlation between SST and winter precipitation zone of Iran, Zones 3,4,6,8 (Regions specified with red frame have PCC > 0.5)

9 to 11, the QBO effect was significant from 1995 to 2013 (see sections 9, 10, and 11 of Fig. 4). While the 36- to 72-month period of the precipitation in zones 5, 7 and 8 were more meaningful (see sections 5, 7 and 8 of Fig. 4). The decadal-like oscillation (around 120 months) was evident in zones 1, 2, 4, and 11. In zones 1, 4, and 11, in some years, the period lasted for 120 months, which can be attributed to the QBO-solar cycle modulation's reciprocal effect (sections 1, 4, and 11 of Fig. 4).

The WTC and XWT were also calculated to determine the prevailing frequencies (or periods) in each zone's precipitation and determine the relationship between the precipitation and SST anomalies. Given the many available maps, some maps are presented in the paper's text, and others are presented in SM (See Figs. SM8 to SM14). For example, the WTC and the XWT for zones 2, 3, 9, and 11 are shown in Figs. 5, 6, 7 and 8.

Figure 5 shows the temporal relationship between the monthly precipitation time series of zone 2 and the SST anomaly of the three oceanic sources. The connection with the North Atlantic Ocean is significant in 16–32 months from 1984 to 2019 in an in-phase mode, which, although outside the COI, can be notable (Fig. 5a). The dominant period in the South Pacific Ocean's WTC plot spans 8–16 months from 2002 to 2008. The straight down arrow shows the SST anomaly of South Pacific leads to winter precipitation anomaly of zone 2 (Fig. 5c). In the XWT map, the same dominant period from 1995 to 2005 is significant. The South Pacific Ocean's predominant period is in the band 8–16 months, especially between 1985 and 2005. However, in the XWT map of the Indian Ocean, it is not impressive despite the three significant periods in WTC (4–8, 8–16, and 16–32 months) in this study's early years (1984–1994).

The XWT and WTC of precipitation zone 3 are presented in Fig. 6. In the North Atlantic Ocean's XWT plot, a significant region from 1996 to 1998 with a 4–8 months period are evident, which shows that the SST anomaly leads to winter precipitation in zone 3 (straight down arrows in the 5% significance level in Fig. 6b). Based on Fig. 6d, a significant region from 1988 to 1999 with an 8–16 months period is evident. The relationship between the Indian Ocean and winter precipitation at this zone was slightly unnoticeable (Fig. 6f). In the South Pacific Ocean's WTC plot, there was a more significant region from 1984 to 2019 with a

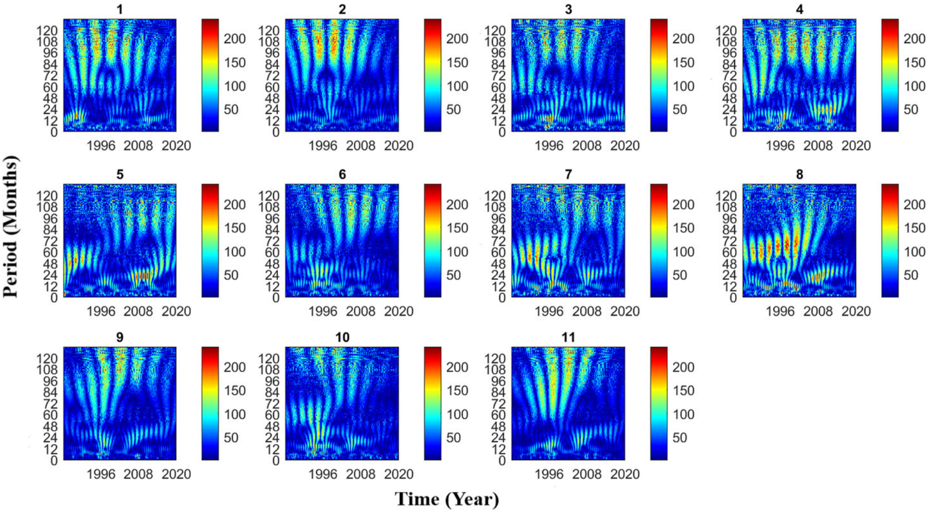

Fig. 4 The CWT of the monthly precipitation anomaly of the 11 different abovementioned zones in Iran

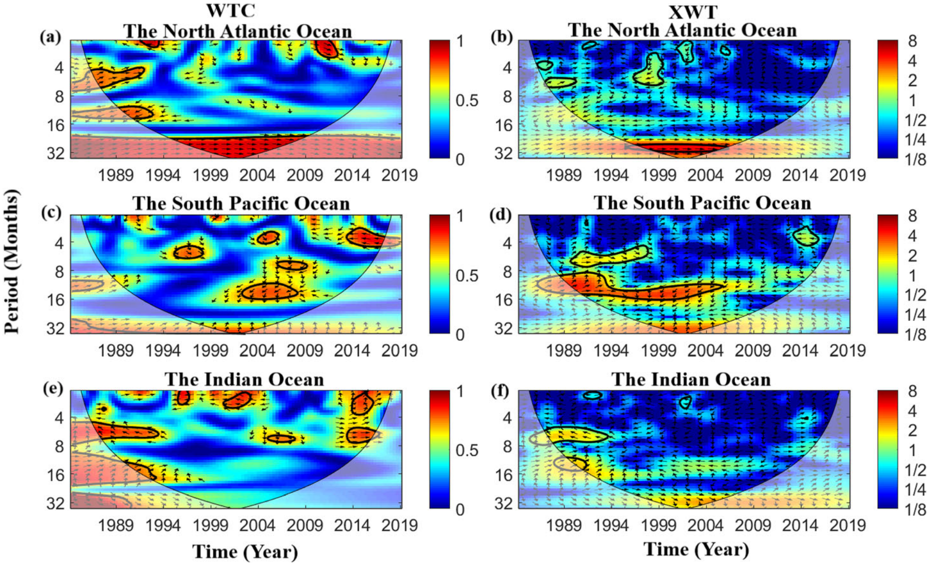

Fig. 5 The WTC (left column) and the XWT (right column) and phase difference between winter precipitation in zone 2 and the oceanic regions (first row for the North Atlantic Ocean, second row for the South Pacific Ocean, and third row for the Indian Ocean). The 5% significance levels are determined with thick black contours; The relative phase relationship is shown as arrows (with in-phase pointing right, anti-phase pointing left)

period of 16–32 months, and a significant region from 1984 to 1995 with an 8–16 months period in an in-phase mode. Most of the areas with 5% significance level were scattered and relatively small in the WTC plots of the Indian Ocean.

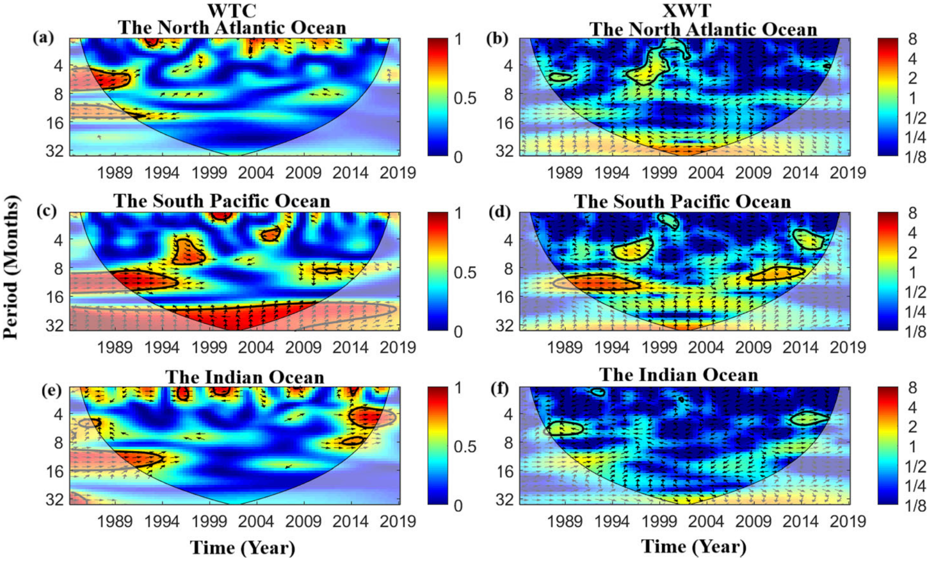

Fig. 6 The WTC (left column) and the XWT (right column) and phase difference between winter precipitation in zone 3 and the oceanic regions (first row for the North Atlantic Ocean, second row for the South Pacific Ocean, and third row for the Indian Ocean). The 5% significance levels are determined with thick black contours; The relative phase relationship is shown as arrows (with in-phase pointing right, anti-phase pointing left)

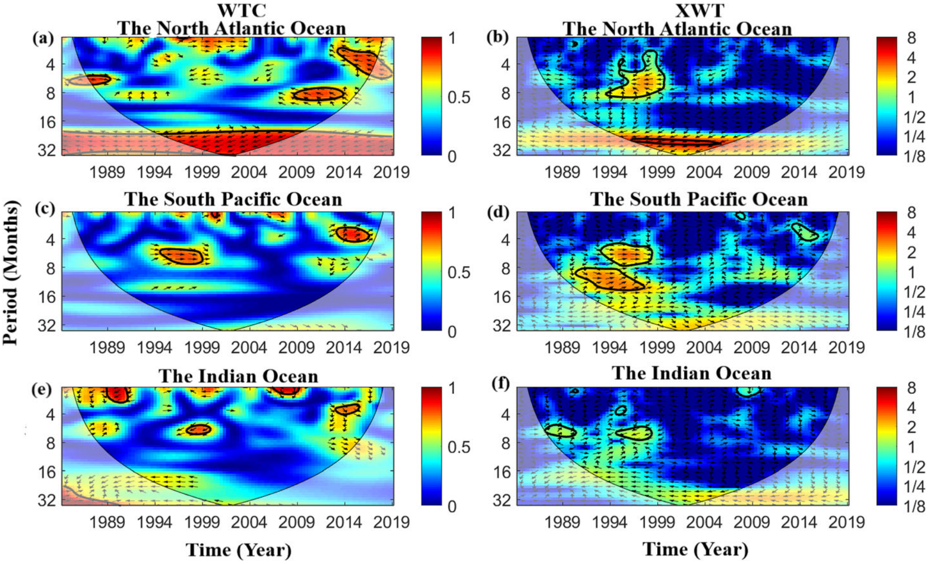

Fig. 7 The WTC (left column) and the XWT (right column) and phase difference between winter precipitation in zone 9 and the oceanic regions (first row for the North Atlantic Ocean, second row for the South Pacific Ocean, and third row for the Indian Ocean). The 5% significance levels are determined with thick black contours; The relative phase relationship is shown as arrows (with in-phase pointing right, anti-phase pointing left)

The largest significant region for the North Atlantic Ocean was observed in the section related to the period of 16 to 32 months in the WTC, with an anti-phase status from 1984 to 2019 (Fig. 7a). In the XWT plot of this ocean, there was a 5% significant region with the same

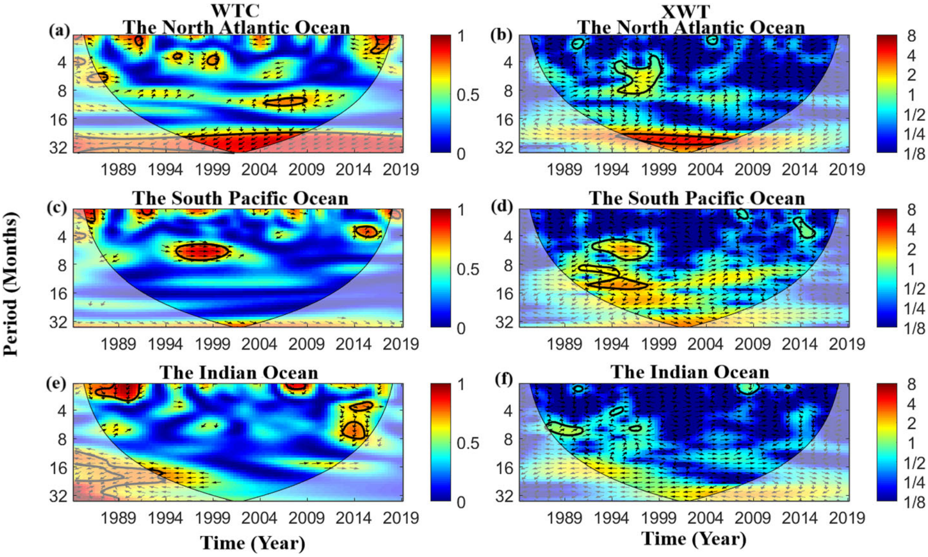

Fig. 8 The WTC (left column) and the XWT (right column) and phase difference between winter precipitation in zone 11 and the oceanic regions (first row for the North Atlantic Ocean, second row for the South Pacific Ocean, and third row for the Indian Ocean). The 5% significance levels are determined with thick black contours; The relative phase relationship is shown as arrows (with in-phase pointing right, anti-phase pointing left)

dominant period from 1997 to 2006. Although from 1990 to 1998 in the XWT plot of the South Pacific Ocean there were two significant 4–8 and 8–16 months period areas with an anti-phase status, such areas were unnoticeable in the Indian Ocean (Fig. 7d, f). Areas with a 5% significance level were scattered and relatively small in the WTC plots for the South Pacific Ocean and the Indian Ocean in precipitation zone 9 (see Fig. 7c, e).

In Fig. 8, the XWT and WTC are specified for SST of oceanic regions and time series of winter precipitation in the 11th zone. Note that there is a large, significant region in the North Atlantic Ocean's WTC plot from 1984 to 2019 with a 16–32 months period in an anti-phase mode (Fig. 8a), which is also repeated in precipitation zones 1, 2 and 9. Also, there was a 5% significant region with the same dominant period from 1997 to 2006 (See Fig. 8b). There were two significant regions in the XWT plot of the South Pacific Ocean with 4–8 and 8–16-month period areas from 1990 to 1998. A continuous significant area of 8–32 months with an in-phase status was observed in the Indian Ocean. Also, a 5% significant region with a 1–4 dominant period from 1987 to 1990 and arrows in the 5% significance level pointing down shows the SST anomaly of this ocean leads to winter precipitation in zone 11 (straight down arrow in Fig. 8e).

As seen in previous studies in Canada, ENSO exerted a relatively strong influence on the winter precipitation (Gan et al. 2007). In previous studies using wavelet analysis, the effect of North Atlantic fluctuations in temperature and rainfall in mid-latitude regions, such as Turkey and the United Arab Emirates, is also evident (Chandran et al. 2016; Sezen and Partal 2020). The most dominant periods, phase difference, and incidence duration for the regions with a 5% significance level (in the WTC and XWT plots) were recognized and listed for all of the studied zones in Tables 2, 3 and 4. The data in these tables help interpret some aspects of the issue. Table 2 indicates that the most extended periods in the WTC plot with a 16–32 months period are in the northwest and southeast part of Iran in zones 1, 2, 9, and 11. Zones 1 and 2 are humid in an in-phase mode, while zones 9 and 11 are arid zones with an anti-phase status. Note that the magnitude of extreme precipitation changes has risen gradually from 1991 through 2010 across the northwest of Iran (Amiri and Mesgari 2018). In the WXT plot, the largest significant region was observed in the 16–32 months period with an anti-phase status from 1994 to 2008, and the smallest significant region was considered in zone 5 (4–8, anti-phase). In zone 10, the largest precipitation zone, the dominant period was not very noticeable. There was no predominant period in the XWT plot, and there was a 5% significant region with a 4–8 months period from 1984 to 1988 in WTC. These tables indicate that the North Atlantic Ocean was the most effective oceanic region for winter precipitation in the west, southwest, and northwest of Iran, but had insignificant impacts in eastern Iran.

Table 3 illustrates the relationship between Iran's precipitation, the North Atlantic SST, and the South Pacific Ocean. For the South Pacific Ocean XWT plot, the predominant periods of 8–16 months were observed throughout Iran, except for zones 7 and 11 in the northeast and southeast. Based on the WTC plot, most of the areas with a 5% significance level were in precipitation zones 2 and 3. The most extended significant region was observed in zones 3, 6, 8, and 10. The relationship between the South Pacific Ocean and precipitation in zone 10, as the most extensive precipitation zone, was noticeable since there was a significant 16–32-month period area from 1984 to 2014, during which the precipitation and this oceanic region were in an in-phase mode. A relevant study showed that the lowest variability in inter-annual and intra-annual precipitation was observed in eastern Iran (Amiri and Mesgari 2017).

Based on Table 4, fewer areas with a 5% significance level were found in the XWT plot for the Indian Ocean. Zones 3 up to 7 and zone 11 had no significant area. The most extended

Table 2 Results of WTC and XWT for the winter precipitation and SST of the North Atlantic Ocean

Zone ID	Years of occurrence (WTC)	Period and phase difference (in months)	Years of occurrence (XWT)	Period and phase difference (in months)
1	(1989–1994); (2009–2012); (1984–2019)	(1–4, anti-phase); (1–4, in-phase); (16–32, in-phase)	(1985–1989)	(4–8, in-phase)
2	(1984–1990); (1984–1990); (1984–2019)	(4–8, in-phase); (8–16, anti-phase); (16–32, in-phase)	(1996–2006)	(16–32, in-phase)
3	(1984–1990); (1984–1992)	(4–8, in-phase); (8–16, anti-phase)	(1996–1999)	(4–8, anti-phase)
4	(1984–1995); (1984–1999)	(4–8, in-phase); (8–16, anti-phase)	(1995–1999)	(4–8, anti-phase)
5	(1984–1991); (2007–2014)	(4–8, in-phase); (8–16, in-phase)	(1998–2001)	(4–8, anti-phase)
6	(1984–1989)	(4–8, in-phase-phase)	(1989–1999)	(8–16, in-phase)
7	(1984–1989); (1994–2001)	(4–8, in-phase)	(1995–1999)	(4–8, anti-phase)
8	(1984–1989); (1992–1998)	(4–8, in-phase); (4–8, anti-phase)	(1996–1999)	(4–8, anti-phase)
9	(2014–2019); (2009–2014); (1984–2019)	(1–4, anti-phase); (4–8, anti-phase); (16–32, anti-phase)	(1993–1999); (1998–2005)	(4–8, anti-phase); (16–32, anti-phase)
10	(1984–1988)	(4–8, in-phase)	–	–
11	(1984–2019)	(16–32, anti-phase)	(1994–2008)	(16–32, anti-phase)

significant region was observed in the 4–8-month period in zones 2 and 10 from 1985 to 1994. The most predominant periods (in the WTC plots) were also detected in precipitation zones 2

Table 3 Results of WTC and XWT for the Winter Precipitation and SST of the South Pacific Ocean

Zone ID	Years of occurrence (WTC)	Period and phase difference (in months)	Years of occurrence (XWT)	Period and phase difference (in months)
1	(1990–1992)	(1–4, in-phase)	(1994–2000)	(8–16, in-phase)
2	(2014–2019); (2003–2009), (1984–1989)	(4–8, anti-phase); (8–16, anti-phase); (16–32, in-phase)	(1986–2005)	(8–16, in-phase)
3	(1995–1999); (1984–1995); (1984–2019)	(4–8, in-phase); (8–16, in-phase); (16–32, anti-phase)	(1988–1998)	(8–16, in-phase)
4	(1994–1998); (1984–2005)	(4–8, in-phase); (16–32, anti-phase)	(1986–2000)	(8–16, in-phase)
5	(1984–1988); (1984–1999)	(4–8, anti-phase); (16–32, anti-phase)	(2009–2014)	(8–16, in-phase)
6	(1984–1988); (1984–2014)	(4–8, anti-phase); (16–32, in-phase)	(1989–1999)	(8–16, in-phase)
7	–	–	(1994–1998)	(4–8, in-phase)
8	(2009–2018); (1984–2014)	(4–8, in-phase); (16–32, anti-phase)	(1996–2002)	(8–16, anti-phase)
9	(2014–2018); (1994–1999)	(1–4, in-phase); (4–8, in-phase)	(1994–1999); (1990–1998)	(4–8, in-phase); (8–16, in-phase)
10	(1984–2014)	(16–32, in-phase)	(1990–1998)	(8–16, in-phase)
11	(1995–2002)	(4–8, in-phase)	(1992–1998)	(4–8, in-phase)

Table 4 Results of WTC and XWT for the winter precipitation and SST of the Indian Ocean

Zone ID	Years of occurrence (WTC)	Period and phase difference (in months)	Years of occurrence (XWT)	Period and phase difference (in months)
1	(1999–2001); (1984–1990)	(1–4, anti-phase); (4–8, anti-phase)	(1984–1990)	(4–8, anti-phase)
2	(2013–2015); (1984–1994); (1984–1993); (1984–1990)	(1–4, anti-phase); (4–8, anti-phase); (8–16, in-phase); (16–32, in-phase)	(1985–1994)	(4–8, anti-phase)
3	(2014–2019); (1984–1994)	(4–8, in-phase); (8–16, in-phase)	–	–
4	(1996–1998); (1984–1991)	(1–4, anti-phase); (4–8, anti-phase)	–	–
5	(2014–2016); (1984–1989); (1984–1990)	(1–4, in-phase); (1–4, anti-phase); (8–16-in-phase)	–	–
6	(2013–2019); (1984–1993)	(4–8, in-phase); (16–32, in-phase)	–	–
7	(2014–2019); (1997–2002)	(4–8, in-phase); (4–8, anti-phase)	–	–
8	(2004–2008); (2010–2015)	(4–8, anti-phase); (8–16, anti-phase)	(1985–1990)	(4–8, in-phase)
9	(1989–1991); (1984–1990)	(1–4, anti-phase); (16–32, in-phase)	(1995–1998)	(4–8, anti-phase)
10	(2007–2009); (2014–2019); (1984–1994); (198–1989)	(1–4, in-phase); (4–8, in-phase); (8–16, anti-phase); (16–32, in-phase)	(1985–1994)	(4–8, in-phase)
11	(1987–1992); (1984–1994)	(1–4, in-phase); (16–32, in-phase)	–	–

and 10. According to Table 3, in recent years (2013–2019), the dominant period of the Indian Ocean and precipitation in Iran is 1–4 and 4–8 months. However, no general regulation can be set for the phase difference between humid, arid, and semiarid zones. Tables 2, 3 and 4 show that different zones behave differently. A general rule cannot be set for any of the zones or zones with the same climate. However, the most effective area for all the zones seems to be the SST of the North Atlantic Ocean and the South Pacific Ocean. Besides, it seems that the 8–16 months period is the most effective and dominant period for all zones.

Figure 9 shows the average percentages of each period (WTC and XWT) for all the studied zones in Iran. In this research, the most effective dominant period was determined based on the duration. For example, there are two significant regions in the WTC plot of the Indian Ocean for zone 8. The period of 4–8 months lasts four years, and a second one, the period of 8–16 months, has a longer duration from 2010 to 2015, so this period was chosen. The most effective and dominant period for WTC of the North Atlantic Ocean is the 4–8 months (36% of all cases), and also in 35% of all cases, 16–32 months period is the dominant period. This WTC percentage is 55% for the South Pacific Ocean and 27% for the Indian Ocean. On the other, the dominant period for the XWT plot of the North Atlantic Ocean lasts 4–8 months observed in 55% of all cases. The XWT of the South Pacific Ocean is an 8–16 months period observed in 81% of precipitation zones. The significant period in the XWT for Indian Ocean is 45% lasting 4–8 months. Six zones in the XWT of the Indian Ocean had shown no relationship (see Table 4).

The maps indicate that the lowest prevailing periods are in the Indian Ocean. The predominant periods in the Indian Ocean remarkably lasted 4–8 months, which is consistent with the seasonal periods. It is clear that the impact of Madden–Julian oscillation (MJO) is between 60 to 90 days. On the other hand, the 8–16 and 16–32 month periods of the South Pacific Ocean represent intra-annual periods, and the North Atlantic Ocean shows inter-annual dominant period (Fig. 9). The obtained results about the dominant period (8–16 months) had relatively good conformity with previous studies that show an intra-annual (0.5–1 year) period on a monthly scale for effects of large-scale climatic indices on precipitation (Chang et al.

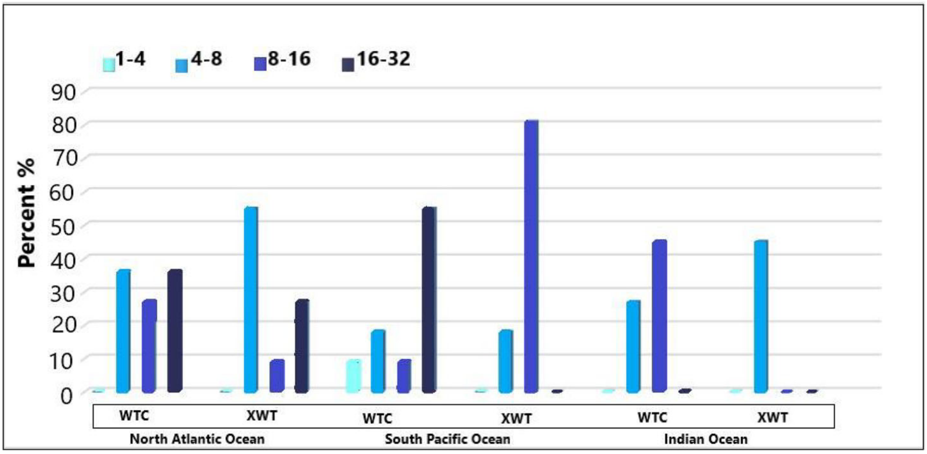

Fig. 9 The average distribution of predominant efficient periods of the oceanic regions in different zones of precipitation in Iran

2019; Nalley et al. 2016; Singh et al. 2020). Previous studies showed that the South Pacific Ocean fluctuations greatly impact precipitation in Iran (Ahmadi et al. 2019; Araghi et al. 2017; Dehghani et al. 2020; Helali et al. 2020; Pourasghar et al. 2012). In present results the South Pacific Ocean's role are outstanding too.

4 Conclusions

A study is presented of a time-frequency linkage between three major oceanic regions, including the North Atlantic, the South Pacific and the Indian Ocean, and winter precipitation (DJF) in Iran between 1984 to 2019 using cross wavelet transform (XWT) and wavelet transform coherence (WTC). The researchers also used the continuous wavelet transform (CWT) to survey for significant periodic characteristics of data series. Based on the results of CWT, in most of Iran's precipitation zones, the El Niño Southern Oscillation effects were apparent. Decadal oscillation is seen in northwestern zones, and the Quasi-Biennial-Oscillation can be clearly seen in zones 5, 7 and 10. The North Atlantic Ocean and the South Pacific Ocean had the most decisive influence on Iran's winter precipitation, as it has most regions with a 5% significance level in the WTC and XWT plots. For all regions, the 8–16 months is the most effective and predominant period based on XWT for the South Pacific Ocean. The most dominant period is the 8–16 months period that can be seen in 81% of all cases. For the North Atlantic Ocean, the dominant period is 4–8 months (55%). There is a less significant relationship between the winter precipitation in Iran and the Indian Ocean despite their proximity. Based on WTC plots, the North Atlantic Ocean dominant periods are 4–8 months (36%) and 16–32 months (36%). The predominant periods for the South Pacific Ocean and the Indian Ocean are respectively 16–32 months (55% of all cases) and 8–16 months (45%). However, recently (2013–2019), the dominant period of the Indian Ocean and precipitation in Iran is 1–4 and 4–8 months. However, studies have shown that the Indian Ocean is known as a source of moisture for the southeast of Iran because of summer precipitation, while this study focuses on winter precipitation in Iran. The results of XWT and WTC represent the seasonal fluctuation of Iran's precipitation related to the Indian Ocean, while the inter-annual oscillation is linked to the North Atlantic Ocean, and the intra-annual fluctuation of precipitation of Iran is relevant to the South Pacific Ocean.

The obtained results about the dominant period (8–16 months) had relatively good conformity with previous studies that show an intra-annual (0.5–1 year) period on a monthly scale for effects of large-scale climatic indices on precipitation. Accordingly, the present results about the dominant period and the South Pacific Ocean's role are prominent. The findings show that the WT can be useful for studying the communication between multiple meteorological time series in a time-frequency space. However, it seems it is better to use longer time series. Longer time series can determine the dominant period with more accuracy. This type of correlative wavelet study can be used in other regions to estimate dominant frequencies and seasonal to decadal oscillation phenomenology.

Supplementary Information The online version contains supplementary material available at https://doi.org/10.1007/s40710-021-00524-0.

Acknowledgments To apply the WTC and XWT methods in this paper, the MATLAB codes used were provided by A. Grinsted (http://noc.ac.uk/using-science/crosswavelet-wavelet-coherence) and C. Torrence and G. P. Compo (http://paos.colorado.edu/research/wavelets/software.html).

Research Data Policy and Data Availability Statements The authors declare that data supporting the findings of this study are available and were cited within the article.

Authors' Contributions Mohammad Joghataei contributed to the study's conception and design. Atefe Ebrahimi performed material preparation, data collection, and analysis. Atefe Ebrahimi and Mohammad Joghataei wrote the first draft of the manuscript, and Dariush Rahimi and Saeed Movahedi commented on the previous versions of the manuscript. All authors read and approved the final manuscript.

Funding The research is part of the Ph.D. thesis of Atefe Ebrahimi and was supported by the University of Isfahan.

Declarations

Conflict of Interest The authors declare that they have no conflict of interest.

References

Ahmadi M, Salimi S, Hosseini SA, Poorantiyosh H, Bayat A (2019) Iran's precipitation analysis using synoptic modeling of major teleconnection forces (MTF). Dynam Atmos Ocean 85:41–56. https://doi.org/10.1016/j.dynatmoce.2018.12.001

Amiri MA, Conoscenti C (2017) Landslide susceptibility mapping using precipitation data, Mazandaran Province, north of Iran. Nat Hazards 89(1):255–273. https://doi.org/10.1007/s11069-017-2962-8

Amiri MA, Mesgari MS (2016) Spatial variability analysis of precipitation in Northwest Iran. Arab J Geosci 9(11):1–10. https://doi.org/10.1007/s12517-016-2611-7

Amiri MA, Mesgari MS (2017) Modeling the spatial and temporal variability of precipitation in Northwest Iran. Atmosphere 8(12):1–14. https://doi.org/10.3390/atmos8120254

Amiri MA, Mesgari MS (2018) Analyzing the spatial variability of precipitation extremes along longitude and latitude, Northwest Iran. Kuwait J Sci 45(1):121–127

Amiri MA, Mesgari MS (2019) Spatial variability analysis of precipitation and its concentration in Chaharmahal and Bakhtiari province, Iran. Theor Appl Climatol 137(3–4):2905–2914. https://doi.org/10.1007/s00704-019-02787-y

Amiri MA, Amerian Y, Mesgari MS (2016) Spatial and temporal monthly precipitation forecasting using wavelet transform and neural networks, Qara-Qum catchment, Iran. Arab J Geosci 9(5):421. https://doi.org/10.1007/s12517-016-2446-2

Amiri MA, Mesgari MS, Conoscenti C (2017) Detection of homogeneous precipitation regions at seasonal and annual time scales, Northwest Iran. J Water Clime Change 8(4):701–714. https://doi.org/10.2166/wcc.2017.088

Araghi A, Baygi MM, Adamowski J, Malard J, Nalley D, Hasheminia SM (2015) Using wavelet transforms to estimate surface temperature trends and dominant periodicities in Iran based on gridded reanalysis data. Atmos Res 155:52–72. https://doi.org/10.1016/j.atmosres.2014.11.016

Araghi A, Mousavi-Baygi M, Adamowski J, Martinez C (2017) Association between three prominent climatic teleconnections and precipitation in Iran using wavelet coherence. Int J Climatol 37(6):2809–2830. https://doi.org/10.1002/joc.4881

Ashraf B, Yazdani R, Mousavi-Baygi M, Bannayan M (2013) Investigation of temporal and spatial climate variability and aridity of Iran. Theor Appl Climatol 118(1):35–46. https://doi.org/10.1007/s00704-013-1040-8

Azad S, Debnath S, Rajeevan M (2015) Analysing predictability in Indian monsoon rainfall: a data analytic approach. Environ Process 2:717–727. https://doi.org/10.1007/s40710-015-0108-0

Baldwin MP, Gray LJ, Dunkerton TJ, Hamilton K, Haynes PH, Randel WJ, Takahashi M (2001) The quasi-biennial oscillation. Rev Geophys 39(2):179–229. https://doi.org/10.1029/1999rg000073

Barbulescu AA (2016) New method for estimation the regional precipitation. Water Resour Manag 30:33–42. https://doi.org/10.1007/s11269-015-1152-2

Bruun JT, Allen JI, Smyth TJ (2017) Heartbeat of the southern oscillation explains ENSO climatic resonances. J Geophys Res Oceans 122(8):6746–6772. https://doi.org/10.1002/2017JC012892

Canchala T, Alfonso-Morales W, Cerón WL, Carvajal-Escobar Y, Caicedo-Bravo E (2020) Teleconnections between monthly rainfall variability and large-scale climate indices in southwestern Colombia. Water 12(7):1863. https://doi.org/10.3390/w12071863

Chandran A, Basha G, Ouarda TBMJ (2016) Influence of climate oscillations on temperature and precipitation over the United Arab Emirates. Int J Climatol 36(1):225–235. https://doi.org/10.1002/joc.4339

Chang X, Wang B, Yan Y, Hao Y, Zhang M (2019) Characterizing effects of monsoons and climate teleconnections on precipitation in China using wavelet coherence and global coherence. Clim Dyn 52:5213–5228. https://doi.org/10.1007/s00382-018-4439-1

Chellali F, Khellaf A, Belouchrani A (2010) Wavelet spectral analysis of the temperature and wind speed data at Adrar, Algeria. Renew Energy 35(6):1214–1219. https://doi.org/10.1016/j.renene.2009.10.010

Chen Y, Guan Y, Shao G, Zhang D (2016) Investigating trends in streamflow and precipitation in Huangfuchuan Basin with wavelet analysis and the Mann-Kendall test. Water 8(3):77. https://doi.org/10.3390/w8030077

Coulibaly P (2006) Spatial and temporal variability of Canadian seasonal precipitation (1900–2000). Adv Water Resour 29(12):1846–1865. https://doi.org/10.1016/j.advwatres.2005.12.013

Coulibaly P, Burn DH (2004) Wavelet analysis of variability in annual Canadian streamflows. Water Resour Res 40(3). https://doi.org/10.1029/2003WR002667

Darand M, Mansouri Daneshvar MR (2014) Regionalization of precipitation regimes in Iran using principal component analysis and hierarchical clustering analysis. Environ Process 1:517–532. https://doi.org/10.1007/s40710-014-0039-1

Das J, Jha S, Goyal MK (2020) On the relationship of climatic and monsoon teleconnections with monthly precipitation over meteorologically homogenous regions in India: wavelet & global coherence approaches. Atmos Res 238:104889. https://doi.org/10.1016/j.atmosres.2020.104889

Dehghani M, Salehi S, Mosavi A, Nabipour N, Shamshirband S, Ghamisi P (2020) Spatial analysis of seasonal precipitation over Iran: Co-variation with climate indices. ISPRS Int J Geoinf 9(2):73. https://doi.org/10.3390/ijgi9020073

Dinpashoh Y (2006) Study of reference crop evapotranspiration in IR of Iran. Agric Water Manag 84(1–2):123–129. https://doi.org/10.1016/j.agwat.2006.02.011

Domroes M, Kaviani M, Schaefer D (1998) An analysis of regional and intra-annual precipitation variability over Iran using multivariate statistical methods. Theor Appl Climatol 61(3–4):151–159. https://doi.org/10.1007/s007040050060

Farajzadeh J, Alizadeh F (2018) A hybrid linear–nonlinear approach to predict the monthly rainfall over the Urmia Lake watershed using wavelet-SARIMAX-LSSVM conjugated model. J Hydroinf 20(1):246–262. https://doi.org/10.2166/hydro.2017.013

Fritier N, Massei N, Laignel B, Durand A, Dieppois B, Deloffre J (2012) Links between NAO fluctuations and inter-annual variability of winter-months precipitation in the Seine River watershed (northwestern France). Compt Rendus Geosci 344(8):396–405. https://doi.org/10.1016/j.crte.2012.07.004

Gan TY, Gobena AK, Wang Q (2007) Precipitation of southwestern Canada: wavelet, scaling, multifractal analysis, and teleconnection to climate anomalies. J Geophys Res Atmos 112(D10). https://doi.org/10.1029/2006JD007157

Grinsted A, Moore JC, Jevrejeva S (2004) Application of the cross wavelet transform and wavelet coherence to geophysical time series. Nonlinear Process Geophys 11:561–566. https://doi.org/10.5194/npg-11-561-2004

Guntu RK, Yeditha PK, Rathinasamy M, Perc M, Marwan N, Kurths J, Agarwal A (2020) Wavelet entropy-based evaluation of intrinsic predictability of time series. Chaos 30(3):033117. https://doi.org/10.1063/1.5145005

Hauke J, Kossowski T (2011) Comparison of values of Pearson's and Spearman's correlation coefficients on the same sets of data. Quaest Geogr 30(2):87–93. https://doi.org/10.2478/v10117011-0021-1

Helali J, Salimi S, Lotfi M, Hosseini SA, Bayat A, Ahmadi M, Naderizarneh S (2020) Investigation of the effect of large-scale atmospheric signals at different time lags on the autumn precipitation of Iran's watersheds. Arab J Geosci 13(18):1–24. https://doi.org/10.1007/s12517-020-05840-7

Hermida L, López L, Merino A, Berthet C, García-Ortega E, Sánchez JL, Dessens J (2015) Hailfall in Southwest France: relationship with precipitation, trends and wavelet analysis. Atmos Res 156:174–188. https://doi.org/10.1016/j.atmosres.2015.01.00

Jiang R, Gan TY, Xie J, Wang N (2014) Spatiotemporal variability of Alberta's seasonal precipitation, their teleconnection with large-scale climate anomalies and sea surface temperature. Int J Climatol 34(9):2899–2917. https://doi.org/10.1002/joc.3883

Kalimeris A, Ranieri E, Founda D, Norrant C (2017) Variability modes of precipitation along a Central Mediterranean area and their relations with ENSO, NAO, and other climatic patterns. Atmos Res 198:56–80. https://doi.org/10.1016/j.atmosres.2017.07.031

Kaplan A, Cane MA, Kushnir Y, Clement AC, Blumenthal MB, Rajagopalan B (1998) Analyses of global sea surface temperature 1856–1991. J Geophys Res Oceans 103(C9):18567–18589. https://doi.org/10.1029/97JC01736

Khalili K, Tahoudi MN, Mirabbasi R, Ahmadi F (2016) Investigation of spatial and temporal variability of precipitation in Iran over the last half century. Stoch Env Res Risk A 30(4):1205–1221. https://doi.org/10.1007/s00477-015-1095-4

Kim S (2004) Wavelet analysis of precipitation variability in northern California, USA. KSCE J Civ Eng 8(4):471–477. https://doi.org/10.1007/BF02829169

Kisi O, Shiri J (2011) Precipitation forecasting using wavelet-genetic programming and wavelet-neuro-fuzzy conjunction models. Water Resour Manag 25(13):3135–3152. https://doi.org/10.1007/s11269-011-9849-3

Komasi M, Sharghi S, Safavi HR (2018) Wavelet and cuckoo search-support vector machine conjugation for drought forecasting using standardized precipitation index (case study: Urmia Lake, Iran). J Hydroinf 20(4):975–988. https://doi.org/10.2166/hydro.2018.115

Kuo CC, Gan TY, Yu PS (2010) Wavelet analysis on the variability, teleconnectivity, and predictability of the seasonal rainfall of Taiwan. Mon Weather Rev 138(1):162–175. https://doi.org/10.1175/2009MWR2718.1

Lee JH, Lee J, Julien PY (2018) Global climate teleconnection with rainfall erosivity in South Korea. Catena 167:28–43. https://doi.org/10.1016/j.catena.2018.03.008

Li F, He L (2017) The effects of dominant driving forces on summer precipitation during different periods in Beijing. Atmosphere 8(3):44. https://doi.org/10.3390/atmos8030044

Mechoso CR, Lyons SW, Spahr JA (1990) The impact of sea surface temperature anomalies on the rainfall over Northeast Brazil. J Clim 3(8):812–826. https://doi.org/10.1175/1520-0442(1990)003<0812:TIOSST>2.0.CO;2

Moazenzadeh R, Mohammadi B, Shamshirband S, Chau KW (2018) Coupling a firefly algorithm with support vector regression to predict evaporation in northern Iran. Eng Appl Comput Fluid Mech 12(1):584–597. https://doi.org/10.1080/19942060.2018.1482476

Moron V, Ward MN, Navarra A (2001) Observed and SST-forced seasonal rainfall variability across tropical America. Int J Climatol 21(12):1467–1501

Muhati FD, Ininda JM, Opijah FJ (2007) Relationship between ENSO parameters and the trends and periodic fluctuations in east African rainfall. J Kenya Meteorol Soc 1(1):20–43

Mwale D, Gan TY, Shen SS, Shu TT, Kim KM (2007) Wavelet empirical orthogonal functions of space-time-frequency regimes and predictability of southern Africa summer rainfall. J Hydrol Eng 12(5):513–523. https://doi.org/10.1061/(ASCE)1084-0699(2007)12:5(513)

Nalley D, Adamowski J, Khalil B, Biswas A (2016) Inter-annual to inter-decadal streamflow variability in Quebec and Ontario in relation to dominant large-scale climate indices. J Hydrol 536:426–446. https://doi.org/10.1016/j.jhydrol.2016.02.049

Nazari-Sharabian M, Karakouzian M (2020) Relationship between sunspot numbers and mean annual precipitation: application of cross-wavelet transform-a case study. J 3(1):67–78. https://doi.org/10.3390/j3010007

Nicholls N (1989) Sea surface temperatures and Australian winter rainfall. J Clim 2(9):965–973. https://doi.org/10.1175/1520-0442(1989)002<0965:SSTAAW>2.0.CO;2

Nourani V, Alami MT, Aminfar MH (2009) A combined neural-wavelet model for prediction of Ligvanchai watershed precipitation. Eng Appl Artif Intell 22(3):466–472. https://doi.org/10.1016/j.engappai.2008.09.003

Obilor EI, Amadi EC (2018) Test for significance of Pearson's correlation coefficient. IJMSS 6(1):11–23

Partal T, Cigizoglu HK (2009) Prediction of daily precipitation using wavelet—neural networks. Hydrol Sci J 54(2):234–246. https://doi.org/10.1623/hysj.54.2.234

Partal T, Kisi O (2007) Wavelet and neuro-fuzzy conjunction model for precipitation forecasting. J Hydrol 342(1–2):199–212. https://doi.org/10.1016/j.jhydrol.2007.05.026

Pathak P, Kalra A, Ahmad S, Bernardez M (2016) Wavelet-aided analysis to estimate seasonal variability and dominant periodicities in temperature, precipitation, and streamflow in the Midwestern United States. Water Resour Manag 30(13):4649–4665. https://doi.org/10.1007/s11269-016-1445-0

Pourasghar F, Tozuka T, Jahanbakhsh S, Sarraf BS, Ghaemi H, Yamagata T (2012) The inter annual precipitation variability in the southern part of Iran as linked to large-scale climate modes. Clim Dyn 39(9–10):2329–2341. https://doi.org/10.1007/s00382-012-1357-5

Qi P, Zhang G, Xu YJ, Wang L, Ding C, Cheng C (2018) Assessing the influence of precipitation on shallow groundwater table response using a combination of singular value decomposition and cross-wavelet approaches. Water 10(5):598. https://doi.org/10.3390/w10050598

Randel WJ, Wu F, Swinbank R, Nash J, O'Neill A (1999) Global QBO circulation derived from UKMO stratospheric analyses. J Atmos Sci 56(4):457–474. https://doi.org/10.1175/1520-0469(1999)056<0457:GQCDFU>2.0.CO;2

Raziei T, Saghafian B, Paulo AA, Pereira LS, Bordi I (2009) Spatial patterns and temporal variability of drought in western Iran. Water Resour Manag 23:439–455. https://doi.org/10.1007/s11269-008-9282-4

Rehman SU, Usmani BA, Khan K, Khan AJ, Ali M, Ahmed A, Ali S (2019) Wavelet analysis for precipitation attributes. IJCSNS 19(4):279

Roushangar K, Alizadeh F (2018) Identifying complexity of annual precipitation variation in Iran during 1960–2010 based on information theory and discrete wavelet transform. Stoch Environ Res Risk Assess 32(5):1205–1223. https://doi.org/10.1007/s00477-017-1430-z

Roushangar K, Alizadeh F, Adamowski J (2018) Exploring the effects of climatic variables on monthly precipitation variation using a continuous wavelet-based multiscale entropy approach. Environ Res 165:176–192. https://doi.org/10.1016/j.envres.2018.04.017

Rousta I, Soltani M, Zhou W, Cheung HH (2016) Analysis of extreme precipitation events over central plateau of Iran. Am J Clim Chang 5:297–313. https://doi.org/10.4236/ajcc.2016.53024

Santos CAG, Galvao CO, Trigo RM, Servat E (2003) Rainfall data analysis using wavelet transform. International Association of Hydrological Sciences Publication 278:195–201

Sattari MT, Apaydin H, Shamshirband S (2020) Performance evaluation of deep learning-based gated recurrent units (GRUs) and tree-based models for estimating ETo by using limited meteorological variables. Mathematics 8(6):972. https://doi.org/10.3390/math8060972

Schneider U, Becker A, Finger P, Rustemeier E, Ziese M (2020) GPCC full data monthly product version 2020 at 0.25°: monthly land-surface precipitation from rain-gauges built on GTS-based and historical data. https://doi.org/10.5676/DWD_GPCC/FD_M_V2020_025. Accessed 1 Mar 2021

Schober P, Boer C, Schwarte LA (2018) Correlation coefficients: appropriate use and interpretation. Anesth Analg 126(5):1763–1768. https://doi.org/10.1213/ANE.0000000000002864

Sezen C, Partal T (2020) Wavelet combined innovative trend analysis for precipitation data in the Euphrates-Tigris basin, Turkey. Hydrol Sci J 65(11):1909–1927. https://doi.org/10.1080/02626667.2020.1784422

Shafaei M, Adamowski J, Fakheri-Fard A, Dinpashoh Y, Adamowski K (2016) A wavelet-SARIMA-ANN hybrid model for precipitation forecasting. J Water Land Dev 28(1):27–36

Shamshirband S, Hashemi S, Salimi H, Samadianfard S, Asadi E, Shadkani S, Kargar K, Mosavi A, Nabipour N, Chau KW (2020) Predicting standardized streamflow index for hydrological drought using machine learning models. Eng Appl Comput Fluid Mech 14(1):339–350. https://doi.org/10.1080/19942060.2020.1715844

Singh A, Thakur S, Adhikary NC (2020) Influence of climatic indices (AMO, PDO, and ENSO) and temperature on rainfall in the northeast region of India. SN Appl Sci 2(10):1–15. https://doi.org/10.1007/s42452-020-03527-y

Smith LC, Turcotte DL, Isacks B (1998) Stream flow characterization and feature detection using a discrete wavelet transform. Hydrol Process 12:233–249. https://doi.org/10.1002/(SICI)1099-1085(199802)12:2<233::AID-HYP573>3.0.CO;2-3

Streten NA (1983) Extreme distributions of Australian annual rainfall in relation to sea surface temperature. Int J Climatol 3(2):143–153. https://doi.org/10.1002/joc.3370030204

Tabari H, Talaee PH (2011) Temporal variability of precipitation over Iran: 1966–2005. J Hydrol 396(3–4):313–320. https://doi.org/10.1016/j.jhydrol.2010.11.034

Tan X, Gan TY, Shao D (2016) Wavelet analysis of precipitation extremes over Canadian ecoregions and teleconnections to large-scale climate anomalies. J Geophys Res Atmos 121(24):14–469. https://doi.org/10.1002/2016JD025533

Torrence C, Compo GP (1998) A practical guide to wavelet analysis. Bull Am Meteorol Soc 79(1):61–78. https://doi.org/10.1175/1520-0477(1998)079<0061:APGTWA>2.0.CO;2

Torrence C, Webster PJ (1999) Interdecadal changes in the ENSO–monsoon system. J Clim 12(8):2679–2690. https://doi.org/10.1175/1520-0442(1999)012<2679:ICITEM>2.0.CO;2

Uvo CB, Repelli CA, Zebiak SE, Kushnir Y (1998) The relationships between tropical Pacific and Atlantic SST and Northeast Brazil monthly precipitation. J Clim 11(4):551–562. https://doi.org/10.1175/1520-0442(1998)011<0551:TRBTPA>2.0.CO;2

van der Ent RJ, Savenije HHG (2013) Oceanic sources of continental precipitation and the correlation with sea surface temperature. Water Resour Res 49:3993–4004. https://doi.org/10.1002/wrcr.20296

Xu Y, Li S, Cai Y (2005) Wavelet analysis of rainfall variation in the Hebei plain. Sci China Ser D-Earth Sci 48(12):2241–2250. https://doi.org/10.1360/04yd0215

Affiliations

Atefe Ebrahimi[1] **· Dariush Rahimi**[1] **· Mohammad Joghataei**[2] **· Saeed Movahedi**[1]

Atefe Ebrahimi
atefe.ebrahimi@gmail.com

Saeed Movahedi
s.movahedi@geo.ui.ac.ir

[1] Department of Physical Geography, Faculty of Geographical Sciences And Planning, University of Isfahan, Isfahan, Iran

[2] Department of Physics, Yazd University, Yazd, Iran